

Computer Simulations of Nonthermal Particles in Clusters of Galaxies: Application to the Coma Cluster

Robert C. Berrington

University of Wyoming

1000 E. University, P. O. Box 3905, Laramie, WY 82072

RBERRING@UWYO.EDU

Charles D. Dermer

Naval Research Laboratory

Code 7653, Washington, DC 20375-5352

DERMER@SSD5.NRL.NAVY.MIL

Abstract

We have developed a numerical model for the temporal evolution of particle and photon spectra resulting from nonthermal processes at the shock fronts formed in merging clusters of galaxies. Fermi acceleration is approximated by injecting power-law distributions of particles during a merger event, subject to constraints on maximum particle energies. We consider synchrotron, bremsstrahlung, Compton, and Coulomb processes for the electrons, nuclear, photomeson, and Coulomb processes for the protons, and knock-on electron production during the merging process. The broadband radio through γ -ray emission radiated by nonthermal protons and primary and secondary electrons is calculated both during and after the merger event. To test the ability of the computer model to accurately calculate the nonthermal emission expected from a cluster merger event, we apply the model to the Coma cluster of galaxies, and show that the centrally located radio emission and the Hard X-ray excess observed at 40-80 keV is well fit by our model. If our model is correct, then the Coma cluster will be significantly detected with GLAST and ground-based air Cherenkov telescopes.

1 Introduction

Merger events between clusters of galaxies are extremely energetic events. The formation history of a cluster of galaxies will include several merger events

(Gabici & Blasi, 2003). With typical masses for a rich cluster $\sim 10^{15} M_{\odot}$, dynamical estimates of the energy deposited in to the internal structure of a cluster is $\sim 10^{63}$ – 10^{64} ergs (Sarazin, 2004). Approximately 5% of the available energy is assumed to accelerate particles from the thermal pool to create a distribution of nonthermal particles. The first-order Fermi process is capable of accelerating particles to $\sim 10^{19}$ eV by the shocks that will form at the interaction boundary of two merging cluster of galaxies (Berrington & Dermer, 2003).

Optical and X-ray studies estimate that ~ 30 – 40% of rich clusters show signs of a current or recent merger event (Forman et al., 1981; Beers, Geller, & Huchra, 1982). Structure formation calculations estimate that a cluster will see several mergers though out its formation history (Lacey & Cole, 1993), indicating that most clusters contain a population of highly energetic nonthermal particles.

Diffuse cluster radio emission with no associated compact counterpart is observed in an ever increasing number of galaxy clusters, providing evidence for the prevalence of diffuse, highly energetic nonthermal particles in galaxy clusters. (Giovannini, Tordi, & Feretti, 1999; Kempner & Sarazin, 2001) The diffuse radio emission is classified in to two categories. Diffuse emission found in the cluster center that mimics the thermal bremsstrahlung emission with random polarization is known as a *radio halo*. Diffuse cluster emission located on the cluster periphery characterized by

irregular shapes and strongly polarized light is known as a *radio relic*. These features are preferentially seen in clusters with current or recent cluster merger events, and are thought to be the observational consequences of nonthermal particles accelerated by shocks formed in a cluster merger event.

2 Models

We present results of a numerical model (Berrington & Dermer, 2003) designed to calculate the time-dependent evolution of nonthermal particle distribution functions evolving through radiative losses. The electrons and are accelerated by the first-order Fermi process and at the shock fronts formed in merging clusters of galaxies, and the resulting photon radiation is calculated. Particle injection functions $Q_{e,p}$ for electrons (“e”) and protons (“p”) are assumed to be described by power-law momentum spectra. In terms of kinetic energy $K_{e,p}$, the injection functions are given by

$$Q_{e,p}(K_{e,p}, t) = Q_{e,p}^0 [K_{e,p}(K_{e,p} + 2m_{e,p}c^2)]^{-\frac{s+1}{2}} (K_{e,p} + m_{e,p}c^2) \exp\left[-\frac{K_{e,p}}{K_{\max}}\right], \quad (1)$$

where s is the injection index and K_{\max} is the maximum particle energy determined by three conditions: the available time to accelerate to a given energy since the formation of the cluster merger event; the requirement that the particle Larmor radius is smaller than the size scale of the system; and the condition that the energy-gain rate through first-order Fermi acceleration is larger than the energy-loss rate due to synchrotron and Compton processes. The constant $Q_{e,p}^0$ normalizes the injected particle function, and is determined by

$$\int_{K_{\min}}^{K_{\max}} dK_{e,p} K_{e,p} Q_{e,p}(K_{e,p}, t) = \frac{\eta_{e,p}}{2} A \eta_{\text{He}}^e m_p v_1^3 \langle n_{\text{ICM}} \rangle, \quad (2)$$

where $\langle n_{\text{ICM}} \rangle$ is the number density of the intra-cluster medium (ICM) averaged over the area A of the shock front, η_{He}^e is an enhancement factor to account for the ions heavier hydrogen, $\eta_{e,p}$ is an efficiency factor taken to be 5% unless otherwise noted, and m_p is the mass of a proton. The minimum kinetic energy K_{\min} is held constant at 10 keV.

The model calculates the forward [v_1] and reverse [v_2] shock speed from the gravitational infall velocity v_g

of a merging cluster. The trajectory of the smaller merging cluster is approximated by a point mass of total mass M_2 that falls onto a dominant cluster of total mass M_1 whose density profile is described by an isothermal beta model. The velocity v of the shock fluid is calculated by solving the equation

$$\frac{\mu_1 n_1}{\mu_2 n_2} = \frac{1 + 3\mathcal{M}_1^{-2}}{1 + 3\mathcal{M}_2^{-2}} \left(\frac{v_g - v}{v}\right)^2, \quad (3)$$

where n_1 and n_2 are the number densities in the dominant and merging cluster, respectively. The mean atomic mass in the dominant cluster and the merging cluster are given by μ_1 and μ_2 , respectively. Both mean atomic masses are set equal to $0.6m_p$.

The Mach speeds of the forward [\mathcal{M}_1] and reverse [\mathcal{M}_2] shocks are calculated by

$$\mathcal{M}_1 = \frac{2}{3} \frac{v}{c_1} \left(1 + \sqrt{1 + \frac{9}{4} \frac{c_1^2}{v^2}}\right),$$

and

$$\mathcal{M}_2 = \frac{2}{3} \frac{v_g - v}{c_2} \left(1 + \sqrt{1 + \frac{9}{4} \frac{c_2^2}{(v_g - v)^2}}\right), \quad (4)$$

where c_1 is the sound speed in the dominant cluster, and c_2 is the sound speed in the merging cluster. The Mach number is defined to be $\mathcal{M}_{1,2} = v_{1,2}/c_{1,2}$ for the forward and reverse shock, respectively. Equation 3 and equation 4 are derived from the shock jump conditions, by equating the energy densities of the forward- and reverse-shocked fluids at the contact discontinuity. Compression ratios C_1 (forward) and C_2 (reverse) are calculated from the equation

$$C_{1,2} = \frac{4}{3(1 - \mathcal{M}_{1,2}^{-2})} \quad (5)$$

The time-dependent particle spectrum $N(K, t)$ is determined from solving the Fokker-Planck equation in energy space, given by

$$\begin{aligned} \frac{\partial N(K, t)}{\partial t} &= \frac{1}{2} \frac{\partial^2}{\partial K^2} [D(K, t) N(K, t)] \\ &\quad - \frac{\partial}{\partial K} [\dot{K}(K, t) N(K, t)] \\ &\quad - \sum_{i=pp,p\gamma,d} \frac{N(K, t)}{\tau_i(K, t)} + Q(K, t). \end{aligned} \quad (6)$$

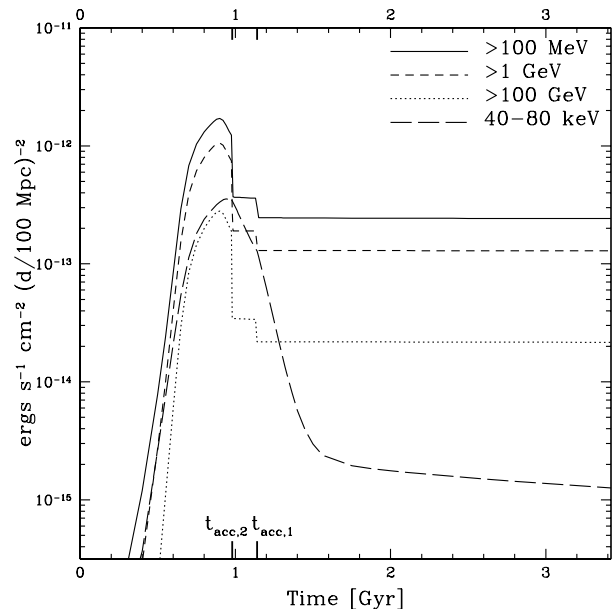
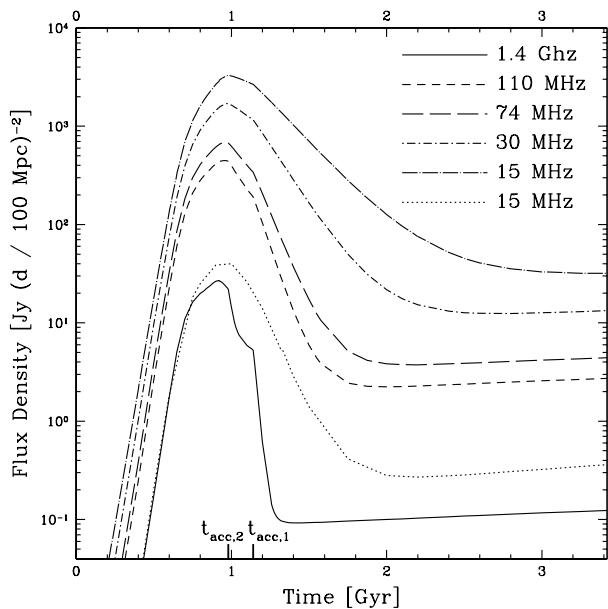


Figure 1: Light curves at various observing frequencies produced by a shock formed in a merger between $10^{14} M_{\odot}$ and $10^{15} M_{\odot}$ clusters that begins at $z_i = 0.3$ and is evolved to the present epoch ($t = 3.42$ Gyr). All light curves are for a magnetic field strength of $B = 1.0 \mu\text{G}$ unless otherwise noted. Radio light curves in Jansky units are given at 15 MHz, 30 MHz, 74 MHz, 110 MHz, and 1.4 GHz. The 15 MHz light curve is also calculated with a magnetic field strength of $B = 0.1 \mu\text{G}$ (dotted curve).

Figure 2: Same as Figure 1 except light curves in energy flux units are given at 40-80 keV, >100 MeV, >1 GeV and >100 GeV. Curves are labeled in the diagram.

Here $\dot{K}(K, t)$ is the total kinetic-energy loss rate found by the sum of Coulomb, synchrotron, bremsstrahlung and Compton processes for electrons, and Coulomb processes for protons. In addition, the protons experience catastrophic losses from proton-proton ($i = pp$) collisions, proton- γ ($i = p\gamma$) collisions, and diffusive escape ($i = d$) on the timescale $\tau_i(K, t)$. Secondary electrons are calculated and added to the primary electron distribution function and are subject to the same energy losses as the primary electrons.

3 Results

Light curves at various observing frequencies are shown in Figures 1 & 2 using the parameters for the standard case of a merger event between a dominant cluster of mass $M_1 = 10^{15} M_{\odot}$, and a merging cluster of mass $M_2 = 10^{14} M_{\odot}$ with a magnetic field strength $B = 1.0 \mu\text{G}$, and a beginning redshift of $z_i = 0.3$. The light curves of the nonthermal radiation exhibit a common behavior independent of frequency. At early times, the spectral power rises rapidly as the clusters

merge. The peak emission occurs when the centers of mass of the two clusters pass at t_{coll} , after which the emission exhibits a slow decay and approaches a plateau at times $t \gtrsim t_{\text{acc}}$. The time $t_{\text{acc},1(2)}$ is defined as the time at which particle injection has terminated at the forward shock (1) or reverse shock (2). The rate of decay of the emission increases with radio frequency due to the stronger cooling of the higher energy electrons, so that the decay is slowest at lower frequencies. Synchrotron emission from secondary electrons forms the late-time plateaus at radio energies. This behavior is also apparent for the hard X-ray emission, although it is formed by primary bremsstrahlung and both primary and secondary Compton radiation at late times. At γ -ray energies, the π^0 -decay emission forms a plateau of emission that dominates soon after t_{acc} .

Calculations of the hardest particle injection spectral index s_{min} formed in cluster merger shocks are shown in Figure 3 as a function of the larger mass M_1 of the two clusters, with a constant subcluster mass $M_2 = 10^{14} M_{\odot}$. We also assume that the onset of the merger begins at redshift $z_i = 0.1$; softer injection indices are obtained for mergers at larger values of z_i because of the smaller maximum separations for merger events occurring at higher redshift. The mean cluster masses are smaller at higher redshift. These lower mass clus-

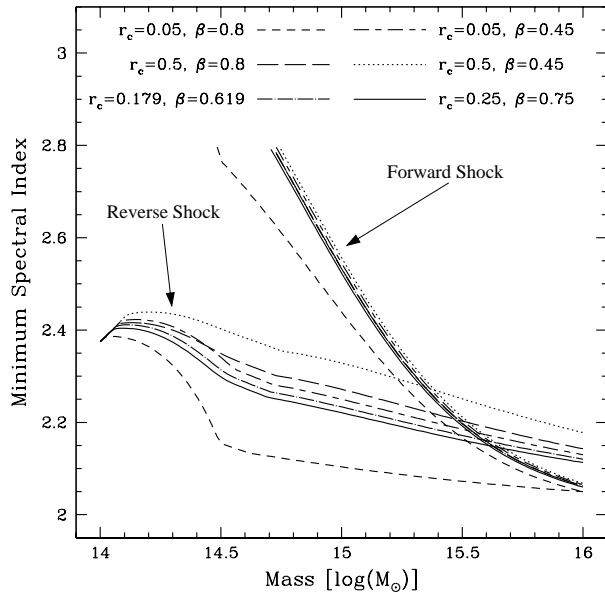


Figure 3: Calculations of the hardest particle injection spectral indices s_{\min} formed in cluster merger shocks as a function of the larger mass M_1 of the two clusters, for various values of r_c and β . The values of r_c are given in Mpc. The minimum spectral index for the forward and reverse shock is shown in the figure.

ters have a lower virial temperature. If this is considered in the calculation of s_{\min} , then it is possible that stronger shocks may be seen at higher redshifts. We calculate s_{\min} for various values of r_c and β . The values $(r_c, \beta) = (0.05, 0.8)$, $(0.05, 0.45)$, $(0.5, 0.8)$, and $(0.5, 0.45)$ roughly correspond to the extrema in the range of these parameters measured for 45 X-ray clusters observed with *ROSAT* (Wu & Xue, 2000). Also shown are values of s_{\min} for $(r_c, \beta) = (0.179, 0.619)$, which are the average values of these parameters for the 45 X-ray clusters, and $(r_c, \beta) = (0.25, 0.75)$, which are the standard parameters used in the calculations. It should be noted that as the dominant cluster approaches the mass of the merging cluster ($10^{14}M_{\odot}$), the spectral indices for the forward and reverse shock will be identical if the matter profiles are identical. However, in Figure 3 the values of (r_c, β) are held constant, and therefore; the matter profiles differ.

3.1 Modeling the Coma Cluster

Both optical (Colless & Dunn, 1996; Biviano et al., 1996; Edwards et al., 2002) and X-ray (Vikhlinin, Forman, & Jones, 1997; Arnaud et al.,

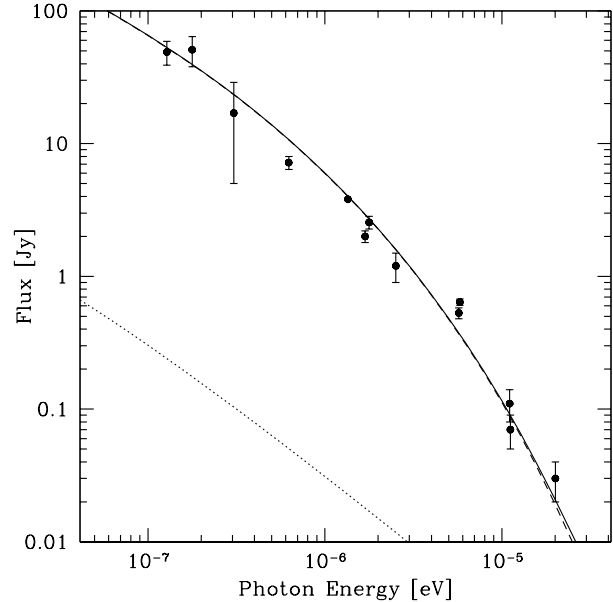


Figure 4: Comparison of radio observations of the Coma cluster with cluster merger shock model. The solid curve is the total expected radio emission, the dashed curve is the contribution to the total emission from primary electrons, and the dotted curve from secondary electrons and positrons. The solid circles are observational data points taken from Thierbach, Klein, & Wielebinski (2003).

2001) observations indicate that the dynamics of the Coma cluster is well-described by a three-body merger model. Colless & Dunn (1996) were the first to find substructure in the central region of Coma that is consistent with a recent merger event near the collision time t_{coll} , defined to be the time when the centers of mass of the two clusters pass through each other. Total mass estimates of the dominant cluster M_1 is estimated to be $0.8 \times 10^{15}M_{\odot}$. X-ray observations (Vikhlinin, Forman, & Jones, 1997) estimate the total mass of the merging cluster M_2 from the gas striped in the merging process to be $\sim 0.1 \times 10^{15}M_{\odot}$. This assumes a gas fraction of 5–10%.

The ICM is well described by an isothermal beta model with core radius $r_c = 0.257$ Mpc, central electron density $\rho_{e0} = 3.82 \times 10^{-3} \text{ cm}^{-3}$, central proton density $\rho_0 = 7.43 \times 10^{-27} \text{ gm cm}^{-3}$, power-law slope $\beta = 0.705$, and a mean gas temperature $\langle T_X \rangle = 8.21$ keV (Mohr, Mathiesen, & Evrard, 1999). The assumed magnetic field strength is $B = 0.22 \mu\text{G}$, and an efficiency factor $\eta_{e,p} = 1\%$. Because we can never know the true gas distribution

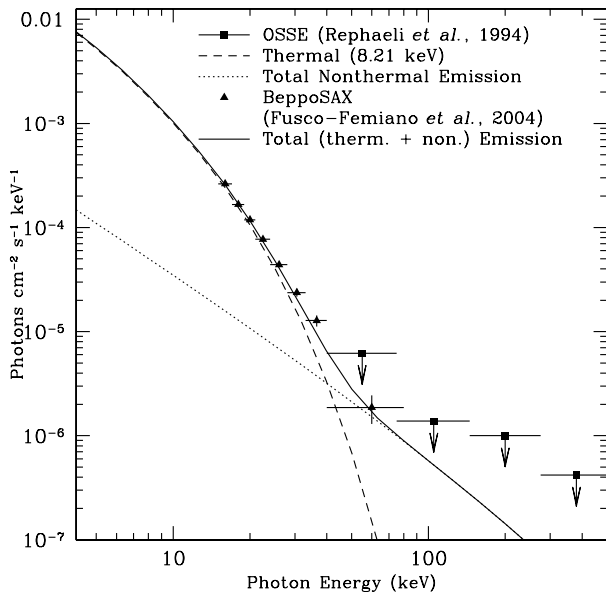


Figure 5: Comparison of X-ray observations of the Coma cluster with the cluster merger shock model. Points are labeled in the diagram. The thermal bremsstrahlung emission (dashed curve) is the calculated thermal bremsstrahlung for the parameters described in the text. The OSSE data points are 2σ upper limits. The solid curve is the sum of the non-thermal (dotted curve) and the thermal 8.21 keV bremsstrahlung emission.

in the merging cluster, we approximate the ICM of the merging cluster by an isothermal beta model with core radius $r_c = 0.150$ Mpc, central electron density $\rho_{e0} = 1.0 \times 10^{-3} \text{ cm}^{-3}$, central proton density $\rho_0 = 1.67 \times 10^{-27} \text{ gm cm}^{-3}$, power-law slope $\beta = 0.7$, and a mean gas temperature calculated from equation 9 in Berrington & Dermer (2003).

The model is evolved to a time $t = 0.97 \times 10^9$ yrs, which is just prior to the collision time $t_{\text{coll}} = 1.0 \times 10^9$ yrs. The redshift of the cluster at the time corresponding to the creation of the shock front corresponds to $z_i = 0.10$ for a $(\Omega_0, \Omega_\Lambda) = (0.3, 0.7)$ cosmology. The observed redshift of the evolved cluster is $z = 0.0232$.

In Figure 4, we show a comparison of our model with the observed radio emission from the radio halo Thierbach, Klein, & Wielebinski (2003). Our models favor a primary electron source for the radio emission from the radio halo. Despite our models using a uniform density profile for the calculation of the secondary electron production, the emission from the sec-

ondary electron is an upper limit to the true secondary electron emission. However, the density in the central region is roughly constant, so that the uniform density assumption is a good approximation to the true secondary electron emission.

In Figure 5, we show a comparison of the calculated thermal and non-thermal emission with the observed Hard X-ray (HXR) emission from the central region of the Coma cluster of galaxies observed by the Phoswich Detection System (PDS) on *BeppoSAX* (Fusco-Femiano et al., 2004). The reported non-thermal photon emission is the total integrated emission expected within 1.5 Mpc of the cluster center. This corresponds to a field of view of $\sim 1^\circ 7$. The PDS has a FWHM field of view of $\sim 1^\circ 3$ which corresponds to a linear scale of ~ 2.2 Mpc. In addition we also show the OSSE 2σ upper limits (Rephaeli, Ulmer, & Gruber, 1994). The HXR emission observed between 20–80 keV is dominated by Compton up scattering of photons off of primary electrons.

The *BeppoSAX*/PDS observations include the merging cluster associated with NGC 4839, and will be contaminated with any non-thermal emission associated with shocks formed in its merging process. The expected non-thermal emission resulting from shocks for a cluster infalling at a minimum distance of $1.6h_{50}^{-1}$ Mpc (Neumann et al., 2001) will be negligible in comparison with the emission from the merger observed in the core of Coma (Berrington & Dermer, 2003).

In Figure 6, we present the predicted γ -ray emission from the Coma cluster of galaxies. The observational limits are taken from Weekes et al. (2002). As seen from the figure, the predicted γ -ray emission falls comfortably below the predicted upper limits for the EGRET observations. Our model predicts that the space-based observatory *GLAST* will detect the non-thermal γ -rays at high significance. Furthermore, we predict that both VERITAS and HESS will have strong $\approx 5\sigma$ detections in 50 hours of observations.

4 Summary and Conclusions

We describe a computer model designed to calculate the nonthermal particle distributions and photon spectra resulting from nonthermal processes produced by shocks that form between merging clusters of galaxies. Over the lifetime of a cluster merger shock $\sim 10^{61}$ – 10^{62} ergs will be deposited in the energy of a nonther-

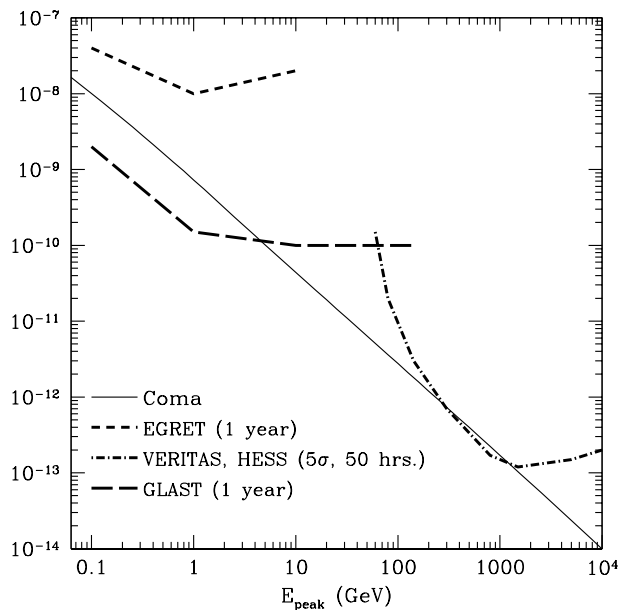


Figure 6: Predicted γ -ray emission from the Coma cluster of galaxies from the cluster merger shock model. The solid curve is the integrated number of particles per cm^2 per s^{-1} greater than E_{peak} . Observational limits for EGRET, *GLAST*, and VERITAS and HESS are included. The EGRET and predicted *GLAST* observational limits are 1 year integrations. The quoted VERITAS and HESS limits are 50 hour, 5σ limits (Weekes et al., 2002). The vertical axis represents the number of particles greater than E_{peak} in units of $\text{cm}^{-2} \text{s}^{-1}$.

mal particle population. From the calculated peak luminosities shown in Figures 1 & 2, we estimate that the nonthermal emission from merger shocks will be detected at radio frequencies with a Long Wavelength Array out to a distance of ~ 2000 Mpc at 15 MHz and ~ 700 Mpc at 120 MHz. At γ -ray energies, we estimate the distance threshold for detection of cluster merger shocks to be ~ 200 Mpc for the space-based observatory *GLAST*. However, each cluster must be considered on a case by case basis to determine its observability.

It was suggested that Galaxy clusters are a dominant contributor to the diffuse extragalactic γ -ray background (DEGB) (Loeb & Waxman, 2000). Our models do not support this claim. Shocks formed in the merger process are weak resulting in a spectral index that is softer than the observed 2.30 ± 0.03 index for the DEGB. The superposition of softer spectra on the harder spectra observed for the most massive merger events will result in a concave spectrum at lower energies that is not observed. We estimate that the contribution to the DEGB by cluster merger shocks will not exceed ~ 1 – 10% .

We applied this model to the Coma cluster of galaxies. We show that the radio emission from the radio halo Coma C is well fit by the cluster merger model. The calculated nonthermal X-ray emission also fits the observed HXR emission observed at 40–80 keV by *BeppoSAX/PDS*. The γ -ray emission expected from this model is also calculated and is shown to fall below the observational limits for EGRET as reported by Reimer et al. (2003), but should be strongly detected by the space-based observatory *GLAST* and the ground-based air Cherenkov telescopes such as VERITAS and HESS. Even though other acceleration mechanisms or point sources could produce nonthermal emission in the core of Coma, our model of cluster merger shocks account for the entire observed radio and HXR emission.

5 Acknowledgments

The work of CD is supported by the Office of Naval Research and *GLAST* Science Investigation Grant No. DPR-S-1563-Y.

References

- Arnaud, M., et al. 2001, *A&A*, 365, L67
- Berrington, R. C. & Dermer, C. D. 2003, *ApJ*, 594, 709

- Biviano, A., Durret, F., Gerbal, D., Le Fevre, O., Lobo, C., Mazure, A., & Slezak, E. 1996, *A&A*, 311, 95
- Beers, T. C., Geller, M. J., & Huchra, J. P. 1982, *ApJ*, 257, 23
- Colless, M. & Dunn, A. M. 1996, *ApJ*, 458, 435
- Edwards, S. A., Colless, M., Bridges, T. J., Carter, D., Mobasher, B., & Poggianti, B. M. 2002, *ApJ*, 567, 178
- Forman, W., Bechtold, J., Blair, W., Giacconi, R., van Speybroeck, L., & Jones, C. 1981, *ApJL*, 243, L133
- Fusco-Femiano, R., Orlandini, M., Brunetti, G., Feretti, L., Giovannini, G., Grandi, P., & Setti, G. 2004, *ApJL*, 602, L73
- Gabici, S. & Blasi, P. 2003, *ApJ*, 583, 695
- Giovannini, G., Tordi, M., & Feretti, L. 1999, *New Astronomy*, 4, 141
- Kempner, J. C. & Sarazin, C. L. 2001, *ApJ*, 548, 639
- Lacey, C. & Cole, S. 1993, *MNRAS*, 262, 627
- Loeb, A. & Waxman, E. 2000, *Nature*, 405, 156
- Mohr, J. J., Mathiesen, B., & Evrard, A. E. 1999, *ApJ*, 517, 627
- Neumann, D. M., et al. 2001, *A&A*, 365, L74
- Reimer, O., Pohl, M., Sreekumar, P., & Mattox, J. R. 2003, *ApJ*, 588, 155
- Rephaeli, Y., Ulmer, M., & Gruber, D. 1994, *ApJ*, 429, 554
- Sarazin, C. L. 2004, (these proceedings)
- Thierbach, M., Klein, U., & Wielebinski, R. 2003, *A&A*, 397, 53
- Vikhlinin, A., Forman, W., & Jones, C. 1997, *ApJL*, 474, L7
- Weekes, T. C. et al. 2002, *Astroparticle Physics*, 17, 221
- Wu, X.-P. & Xue, Y.-J. 2000, *ApJ*, 542, 578